Science of the Total Environment 849 (2022) 157785

Contents lists available at ScienceDirect

Science of the Total Environment

journal homepage: www.elsevier.com/locate/scitotenv

Summer ozone pollution in China affected by the intensity of Asian monsoon systems

Yang Zhou [a], Yang Yang [a,*], Hailong Wang [b], Jing Wang [c], Mengyun Li [a], Huimin Li [a], Pinya Wang [a], Jia Zhu [a], Ke Li [a], Hong Liao [a]

[a] Jiangsu Key Laboratory of Atmospheric Environment Monitoring and Pollution Control, Jiangsu Collaborative Innovation Center of Atmospheric Environment and Equipment Technology, Nanjing University of Information Science and Technology, Nanjing, Jiangsu, China
[b] Atmospheric Sciences and Global Change Division, Pacific Northwest National Laboratory, Richland, WA, USA
[c] Tianjin Key Laboratory for Oceanic Meteorology, Tianjin Institute of Meteorological Science, Tianjin, China

HIGHLIGHTS

- East and South Asian summer monsoon have different positive/negative effects on ozone concentration in China.
- Asian summer monsoon mainly affects ozone by changing transboundary transport related to large-scale circulation variations.
- The sustainable and medium development scenarios are the perfect pathways to mitigate ozone pollution.
- High social vulnerability and radiative forcing scenarios can enhance future ozone pollution in China.

GRAPHICAL ABSTRACT

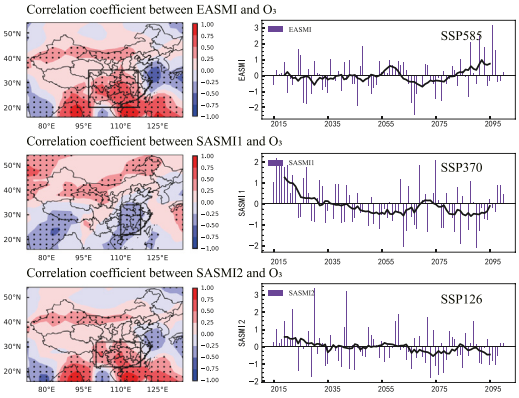

ARTICLE INFO

Editor: Pingqing Fu

Keywords:
Ozone
Asian summer monsoon
China
Transboundary transport
Future projection

ABSTRACT

Ozone in the troposphere is harmful to human health and ecosystems. It has become the most severe air pollutant in China. Here, based on global atmospheric chemistry model simulations during 1981–2019 and nation-wide surface observations, the impacts of interannual variations in Asian summer monsoon (ASM), including East Asian summer monsoon (EASM) and South Asian summer monsoon (SASM), on surface O_3 concentrations during June-July-August (JJA) in China are investigated. EASM intensity has a significant positive correlation with the surface O_3 concentration in south-central China (97.5°–117.5°E, 20°–35°N) with a correlation coefficient of 0.6. Relative to the weak EASM years, O_3 concentrations in strong EASM years increased by up to 5 ppb (10 % relative to the average) due to the weakened transboundary transport of O_3 resulting from the decrease in prevailing southwesterlies. SASM can be divided into two components. The one near East Asia has a similar relation with O_3 in southern China (100°–117.5°E, 22°–32°N) as that of EASM. The other component of SASM is negatively correlated with surface O_3 concentration in eastern China (110°–117.5°E, 22°–34°N) and the maximum difference in O_3 concentrations exceeded 5 ppb (10 %) between the strong and weak monsoon years, which can be explained by the O_3 divergence caused by the anomalous southerlies blowing pollutants away from the northern boundary of eastern China. This study shows that the ASM has an important impact on the O_3 concentrations in China, primarily through changing transboundary transport related to the variability of large-scale circulations, which has great implications for air pollution prevention and mitigation in China. Future projections of ASM suggests that the sustainable and medium development scenarios are the

* Corresponding author.
E-mail address: yang.yang@nuist.edu.cn (Y. Yang).

http://dx.doi.org/10.1016/j.scitotenv.2022.157785
Received 14 June 2022; Received in revised form 29 July 2022; Accepted 29 July 2022
Available online 3 August 2022

perfect pathways that can help to mitigate O_3 pollution, while high social vulnerability and radiative forcing scenarios could enhance future O_3 pollution in China.

1. Introduction

Tropospheric Ozone (O_3), one of the most important oxidants in the air, is produced by a series of photochemical reactions between nitrogen oxides (NO_x) and volatile organic compounds (VOCs) when exposed to sunlight (Li et al., 2021; Fu et al., 2019). High concentrations of O_3 harm human health, leading to increased morbidity and mortality worldwide (Chen et al., 2018; Malley et al., 2017). Leaves of plants can be damaged by O_3 through reducing the rate of photosynthesis, which leads to disruptions in the carbon and water cycles (Ainsworth et al., 2012; Emberson et al., 2018; Mills et al., 2018). In recent years, O_3 pollution has become the most concerning pollutant in China (Fu et al., 2019; Gao et al., 2020; Li et al., 2021). The daily maximum 8 h average O_3 concentration in summer increased at a rate of 5 % per year in the last decade (Lu et al., 2020). Hence, studying the factors that affect the summertime O_3 concentrations in China is essential to guiding O_3 pollution control and achieving the goal of healthy air quality in the near future.

Climate in China is significantly dominated by the Asian monsoon system (Steinke et al., 2006; He et al., 2007). As one of the sub-systems of the Asian summer monsoon (ASM), the East Asian Summer Monsoon (EASM) brings clean, warm and humid air from the ocean to eastern China. The variabilities in EASM have been reported to exert a non-negligible impact on the O_3 variation in China (Li et al., 2017; Liu et al., 2019; Yang et al., 2014; Zhao et al., 2010; Zhou et al., 2013). Yang et al. (2014) investigated the interannual variation in summertime O_3 concentrations in China during 1986–2006 based on GEOS-Chem simulations and found that they were largely affected by the strength of EASM, with O_3 concentration in the strong EASM years higher than that in the weak EASM years by 6 % over central and northeastern China. Their sensitivity simulations indicated that the higher O_3 concentrations in the strong EASM years were mainly due to the difference in O_3 transboundary transport related to the changes in large-scale circulation. Li et al. (2017) used the regional climate model RegCM4-Chem to explore the impacts of the EASM intensity on O_3 concentrations between 1999 and 2013 and found that relative to weak EASM year, O_3 concentrations during the strong EASM years increased over central and northeastern China and decreased over eastern China with changes in the range of -4 to 4 ppb (parts per billion), which is consistent with Yang et al. (2014). However, based on IPR analysis, they revealed that the O_3 differences were primarily related to the chemical processes influenced by the varying shortwave radiation and temperature.

Before nation-wide observational network started measuring surface O_3 concentrations, earlier ground-based measurements at limited sites also exhibit a correlation between EASM and O_3 in China. Xu et al. (2018) reported a negative correlation between EASM and O_3 concentration in July at Mt. Waliguan Observatory on Tibetan Plateau over 1994–2013 due to changes in stratospheric O_3 injection and atmospheric circulation. Zhou et al. (2013) investigated the relationship between EASM and O_3 at Hong Kong Observatory over the southern coastal region of China during 2000–2010 and pointed out the importance of monsoon in affecting the interannual variation of lower tropospheric O_3 concentrations.

Due to the lack of observational data, most studies previously examining the impact of EASM on O_3 in China used model simulations alone or observations at limited sites. Moreover, as another important subsystem of the ASM (Ding and Chan, 2005), the South Asian summer monsoon (SASM) also potentially affects the interannual variation in O_3 concentrations in China (Yin et al., 2017), which was rarely analyzed in previous studies.

This study is extended from Yang et al. (2014), which explored the impact of EASM alone on O_3 in China during 1986–2006 purely depending on model simulations. In this study, we investigate the influences of both EASM and SASM on summertime O_3 concentrations in China over 1981–2019 and the underlying mechanisms based on both observations and model simulations. In addition, the future trends of EASM and SASM under various climate scenarios over 2015–2100 are also presented, using multi-model results from the Coupled Model Intercomparison Project Phase 6 (CMIP6), to explore the future variations in O_3 concentrations over China influenced by the ASM systems. This study provides a deep understanding of the relationship between atmospheric environment and climate systems, which is of great significance for air pollution mitigation and control in China.

2. Methods

2.1. Model description and experimental design

Ozone concentrations are simulated in this study using the global atmospheric chemistry model GEOS-Chem (version v12.9.3), which is driven by the Modern-Era Retrospective analysis for Research and Application, Version 2 (MERRA-2). We use 47 vertical layers from the surface to 0.01 hPa and a horizontal grid of 2° latitude × 2.5° longitude. The model has a fully coupled O_3-NO_x-hydrocarbon-aerosol chemistry mechanism (Pye et al., 2009; Mao et al., 2013; Sherwen et al., 2016). Boundary layer mixing uses the nonlocal scheme (Lin and McElroy, 2010) and stratospheric O_3 chemistry employs the LINOZ scheme (McLinden et al., 2000). GEOS-Chem can archive multiple physical and chemical processes of various tracers during its simulation, which is useful for quantifying the individual processes causing the O_3 variation.

The global anthropogenic emissions used in this study are from the Community Emissions Data System (CEDS, Hoesly et al., 2018) and the Biomass burning emissions are from the Global Fire Emissions Database version 4 (GFED4, van der Werf et al., 2017). Offline emissions from biogenic sources are provided by the Model of Emissions of Gases and Aerosols from Nature version 2.1 (MEGAN V2.1, Guenther et al., 2012). Emissions from lightning and soil are prescribed to the model (Hudman et al., 2012; Ott et al., 2010). Anthropogenic emissions of O_3 precursor gases in China are updated to the Multi-resolution Emissions Inventory (MEIC), which is a localized emission data set in China. The simulated O_3 distribution with the same configuration in GEOS-Chem has been widely assessed in many studies, and the model has been reported to well capture the O_3 concentrations in China (e.g., Li et al., 2019; Lu et al., 2019a, 2019b; Ni et al., 2018).

O_3 concentrations from 1981 to 2019 are simulated from the GEOS-Chem model driven by the time-varying MERRA-2 meteorological fields. Anthropogenic, biomass burning, biogenic and other natural emissions are held at 2017 levels during the simulations, as 2017 is the last year of MEIC inventory for public release and is close to current emission level, thus removing the effects of emission changes on the interannual variation of O_3. However, we also note that fixing emissions at a certain year can have a small effect on the seasonal mean O_3 concentrations, but it does not introduce large biases in our qualitative analysis for the influencing mechanism of Asian summer monsoon on O_3 in China. The influence of monsoon intensity on the interannual changes in O_3 over China in summer can be quantitatively studied using the simulations driven by realistic meteorology.

2.2. CMIP6 multi-model data

To explore the future trend of Asian summer monsoon, multi-model data of zonal and meridional wind fields from 19 models listed in Table S1 with four future scenarios for the Shared Socioeconomic Paths (SSPs, including SSP1-2.6, SSP2-4.5, SSP3-7.0 and SSP5-8.5) of CMIP6 were used. The

monsoon indices are calculated using the multi-model mean data to investigate the future changes in O_3 concentrations in China caused by the variations in monsoon systems.

2.3. Observational ozone data

To evaluate the relationship between ASM and O_3 in China simulated in GEOS-Chem model, surface O_3 concentration data (2014 to 2020) from China National Environmental Monitoring Center (CNEMC) are used in this study. Seasonal mean O_3 concentrations in JJA at 940 sites are analyzed to explore the impact of ASM on O_3. However, it should be noted that only 7 years of observational data are available, which could cause sample bias in the relationship. Also, the changes in emissions during the analysis period may obscure the effect of ASM.

2.4. Monsoon indices

Monsoon indices are used to characterize the year-to-year variation of the monsoon. In this study, the EASM Index and SASM index are calculated based on Li and Zeng (2002). EASM index is defined as the seasonal mean dynamic normalized seasonality (DNS), a function of zonal and meridional winds from reanalysis or model results, over the EASM region (110°–140°E, 10°–40°N) in June-July-August (JJA). Two independent components, SASM1 and SASM2 indices are included in the SASM index, which are estimated in this study as the mean DNS for the two SASM sub-systems (35°–70°E, 2.5°–20°N and 70°–110°E, 2.5°–20°N), respectively, from June to August and have different linkages with the SASM precipitation. The DNS is defined as:

$$\delta_{m,n} = \frac{\|\overline{V_1} - V_{m,n}\|}{\|\overline{V}\|} - 2$$

where m and n denote month and year, respectively. $\overline{V}_1$ and $V_{m,n}$ are the January climatological and monthly wind vectors in a grid box, respectively, and $\overline{V}$ is the mean of January and July climatological wind vectors at the same grid. The norm $\|V\|$ is calculated as $\|V\| = (\iint_s |V|^2 dS)^{1/2}$, where S represents the domain of integration. The monsoon regions are shown in Fig. 1. Positive values of EASM and SASM indices represent strong monsoon years and negative values represent weak monsoon years.

2.5. IPR analysis method

Integrated process rate (IPR) analysis is used to assess the contribution of individual chemical or physical processes to the production and distribution of atmospheric pollutants per unit time in the study domain. The major processes affecting O_3 concentration contain chemical reaction, horizontal advection, vertical convection, dry deposition and diffusion. IPR analysis has been widely applied to identify key processes conducive to extreme air pollution events as well as interannual and decadal variations of air pollutants (Mu and Liao, 2014; Lou et al., 2015; Shu et al., 2016; Yang et al., 2022).

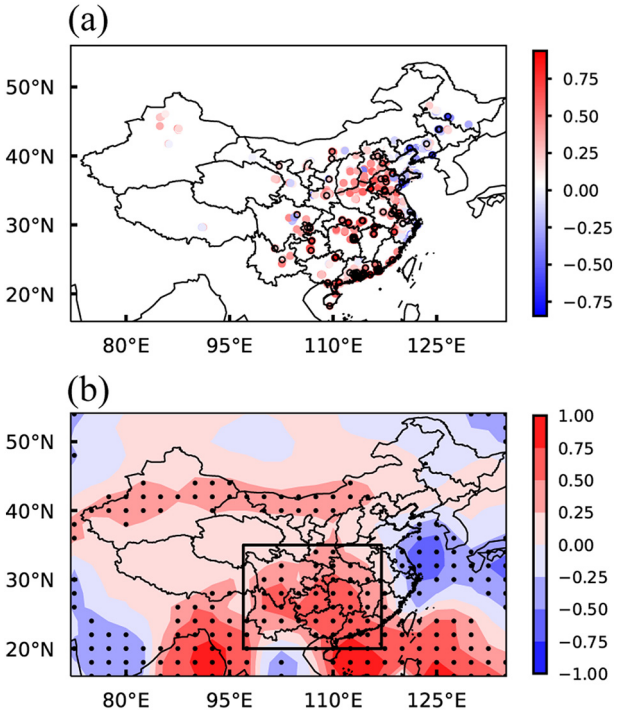

Fig. 2. Spatial distribution of correlation coefficients between EASM index and (a) observed (2014–2020) and (b) simulated (1981–2019) JJA mean surface ozone concentrations. Sites with solid circle outlines in (a) and dotted areas in (b) indicate statistical significance with 90 % confidence. Boxed area marks south-central China (97.5°–117.5°E, 20°–35°N).

3. EASM intensity affects ozone in China

In order to study the relationship between EASM and O_3 interannual variation in China, the correlation coefficient distributions of surface O_3 concentrations and EASM index in JJA based on observations and simulations are shown in Fig. 2. The modeling results show that significant positive

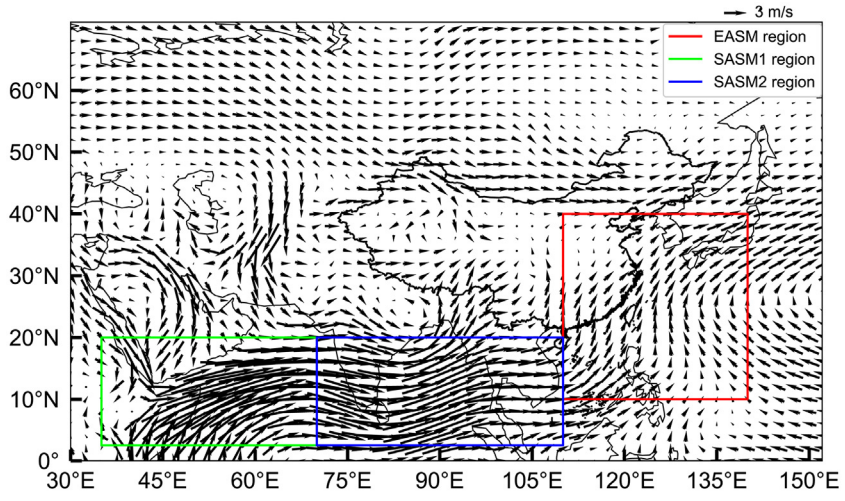

Fig. 1. Spatial distribution of June-July-August mean wind fields at 850 hPa averaged over 1981–2019. Coloured boxes (red/green/blue) represent different monsoon regions (EASM/SASM1/SASM2).

correlation coefficients are located over central and southern China and negative values appear in the coastal areas of eastern China and East China Sea during 1981–2019. Surface measurement data also support the positive relationship between the EASM index and JJA O_3 in China, with 95 % (313 out of 329) sites presenting positive correlation over south-central China (97.5°–117.5°E, 20–35°N), although the observations only cover years of 2014–2020. The correlation coefficient between the EASM index and regional mean modeled JJA O_3 concentration averaged over south-central China is 0.60 (Fig. S1). Given that the emissions of O_3 precursors are kept at 2017 levels during the model simulations, the strong positive correlation suggests that the EASM intensity has large influences on O_3 concentrations and summertime O_3 concentrations are higher (lower) than normal in strong (weak) EASM years over south-central China.

Fig. 3 shows the composite differences in JJA surface O_3 concentrations between the five strongest EASM years and the five weakest EASM years during 1981–2019, to illustrate the effect of EASM on surface O_3 in China. The O_3 level was generally higher in China during the strongest EASM years, with the maximum difference over 5 ppb (10 % relative to the average) over south-central China, compared with the weakest EASM years. In addition, the anomalous O_3 increase over south-central China during the strong EASM years extends from the surface to 300 hPa along 100°–115°E. The impact of EASM on O_3 in China becomes increasingly pronounced from June to August (Fig. S2). The positive differences in O_3 concentrations between the strongest and weakest EASM years reach the maximum in August by >10 ppb (20 %) over south-central China, which is in agreement with Li et al. (2017) using the regional model RegCM4-Chem.

To explore the underlying mechanisms explaining the EASM impact on O_3 levels in China, we quantify the changes in various meteorological parameters in JJA between the five strongest and five weakest EASM years, as shown in Fig. 4. During the strong EASM years, the western Pacific Subtropical High (WPSH) is weakened (Wang et al., 2013), accompanied by abnormal northeasterlies appearing in south-central China (Fig. 4a and b). The weakened prevailing southwesterlies result in less import of clean and moist air from the ocean and consequently reduce the export of polluted air out of the continent, which lead to the O_3 accumulation in south-central China (Yang et al., 2022). It can be further proved through the IPR analysis given in Table 1. Horizontal transport is the only net gain process (23.76 Gg day^{-1}) that leads to the increase in tropospheric O_3 level in south-central China in summer. In general, O_3 is transported out through the east boundary of south-central China. During strong EASM years, the export of O_3 out to the east from the surface to 500 hPa is reduced by 11.96 Tg, compared to the weak EASM years (Table 2), which is significantly larger than the changes in O_3 mass through the other boundaries, leading to the O_3 convergence in this region.

With strong downwelling shortwave radiation and low cloud fraction in the strong EASM years relative to weak EASM years over south-central China, the chemical production of O_3 is tend to increase. However, compared to the weak EASM years, strong EASM years are accompanied by a lower temperature and higher humidity (Fig. 4d, e and g), which are not conducive to the chemical production of O_3 (Gong et al., 2020). The overall O_3 chemical production is reduced. This is also confirmed by the decrease in net O_3 change in the chemical reaction process (−18.97 Gg day^{-1}) between the five strongest and five weakest EASM years (Table 1). Therefore, the EASM influences O_3 concentrations over south-central China mainly through changing the transboundary transport of O_3 instead of perturbing the chemical production.

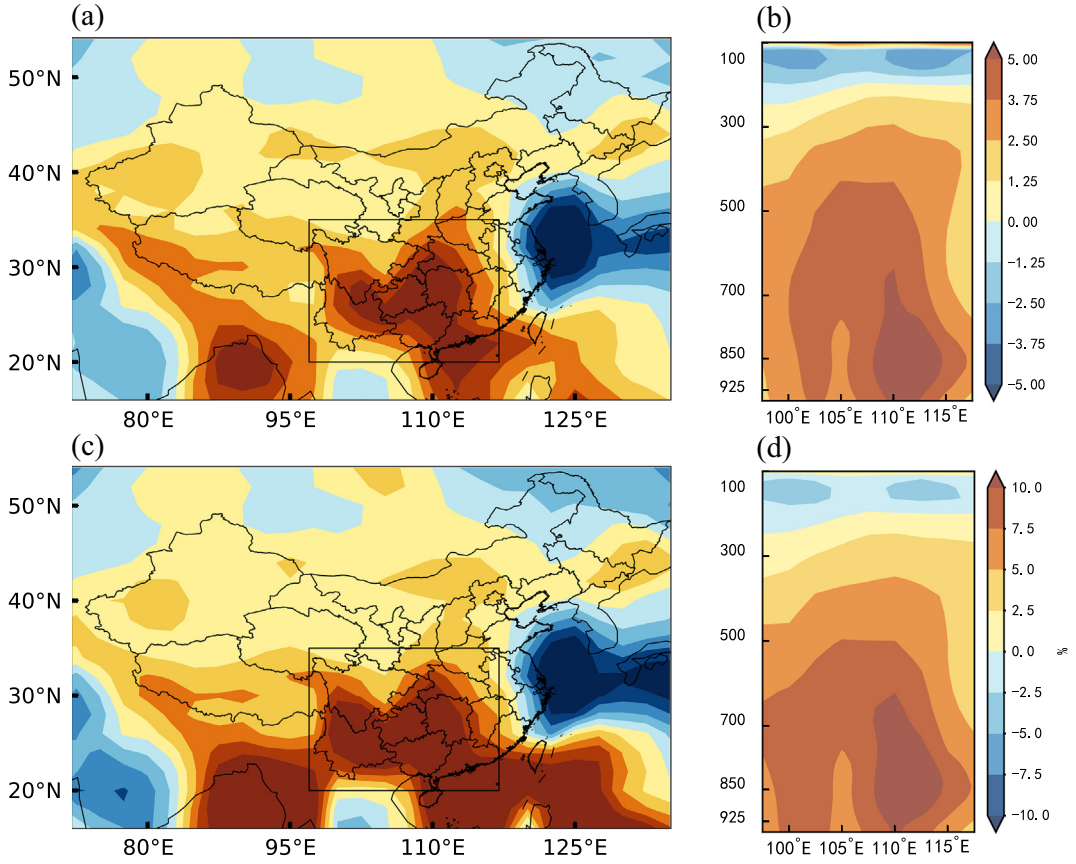

Fig. 3. Horizontal distributions of absolute (ppb, a) and percentage (%, c) differences in JJA surface O_3 concentrations between the selected five strongest (1985, 1997, 2002, 2012 and 2018) and five weakest EASM years (1988, 1996, 1998, 2010 and 2017) (strongest minus weakest). Pressure–longitude cross sections averaged over 20°–35°N for absolute (ppb, b) and percentage (%, d) differences in JJA O_3 concentrations between the selected five strongest and five weakest EASM years (strongest minus weakest). Boxed area marks south-central China.

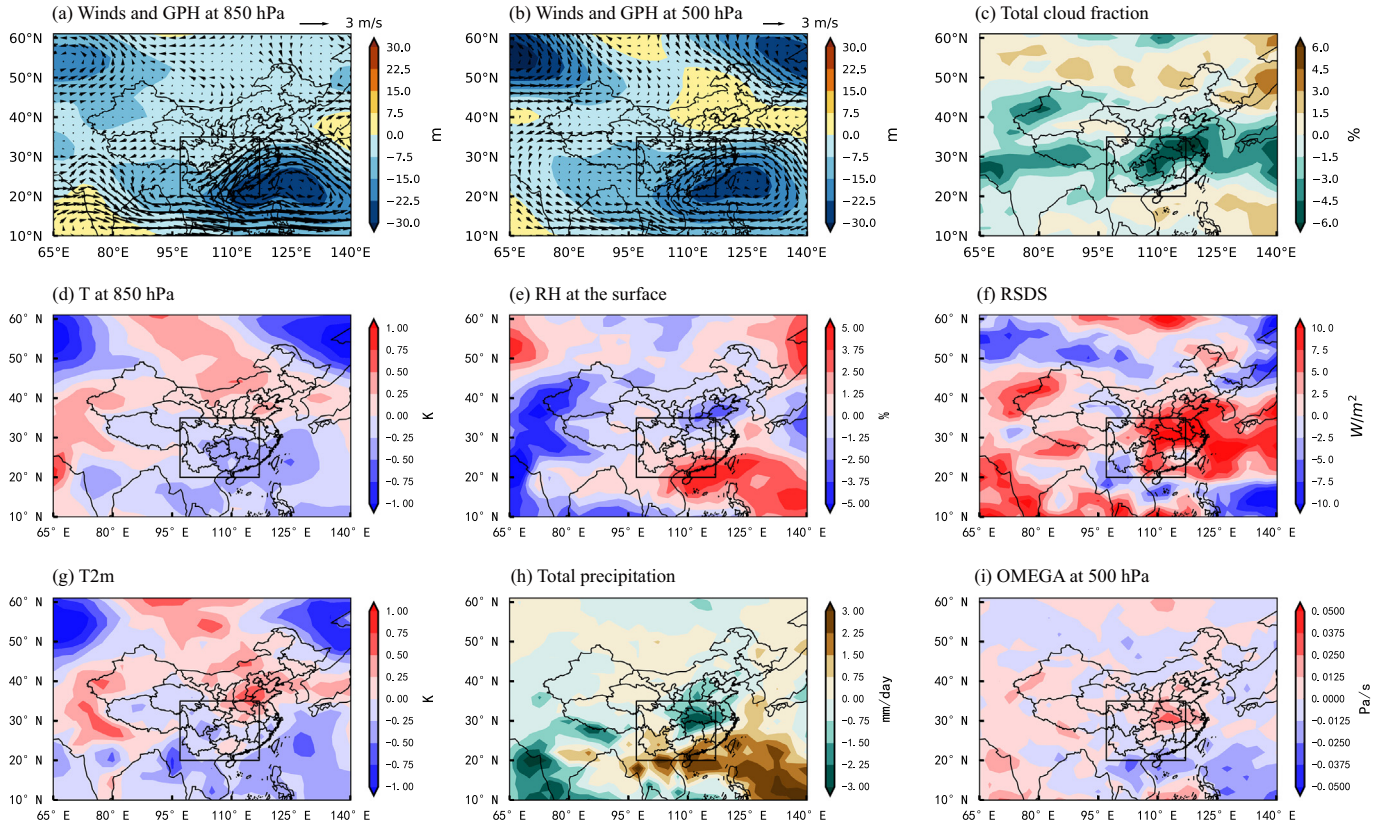

Fig. 4. The composite differences in wind fields (m s^{-1}, vector) and geopotential height (GPH, m, contour) at (a) 850 hPa and (b) 500 hPa, (c) total cloud fraction (%), (d) air temperature (T, K) at 850 hPa, (e) relative humidity (RH, %) at the surface, (f) downwelling shortwave radiation at the surface (RSDS, W m^{-2}), (g) 2-meter air temperature (T2m, K), (h) precipitation rate (mm day^{-1}), and (i) vertical pressure velocity (OMEGA, Pa s^{-1}) between five strongest and five weakest EASM years (strongest minus weakest). Boxed area marks south-central China.

Table 1
Differences in net rate of changes in tropospheric O_3 mass (Gg day^{-1}) in JJA over south-central China (97.5°–117.5°E, 20°–35°N), eastern China (110°–117.5°E, 22°–34°N) and southern China (100°–117.5°E, 22°–32°N) due to physical and chemical processes between the five strongest and the five weakest EASM, SASM1 and SASM2 years, respectively. Note that, the differences in convective transport of O_3 mass at the top of the troposphere are <0.01 Gg day^{-1} and thus not shown.

	South-central China (EASM)	Eastern China (SASM1)	Southern China (SASM2)
Chemical reaction	−18.97	5.16	−6.21
Net horizontal transport	23.76	−6.84	9.07
Diffusion/dry deposition	−4.58	1.06	−1.88

4. SASM intensity affects ozone in China

4.1. Impacts of interannual variation in SASM1

As another component of the ASM, SASM significantly interacts with EASM (Ding and Chan, 2005) and can also affect O_3 variations in China. Due to the existence of two independent components of the SASM, SASM1 and SASM2, their impacts on O_3 in China are analyzed separately.

Fig. 5 shows correlation coefficients between SASM1 index and O_3. The SASM1 index shows a relatively weak but significant negative correlation (−0.25 to −0.5) with JJA surface O_3 concentrations over eastern China (110–117.5°E, 22–34°N) during 1981–2019 simulated by GEOS-Chem (Fig. 5b). The limited observational O_3 data during 2014–2020 also support the model results, with 84 % (141 out of 168) sites in eastern China having negative correlation coefficients (Fig. 5a). Averaged over eastern China, the correlation coefficient between surface O_3 concentrations and SASM1 index is −0.40 (Fig. S3), implying that SASM1 has an important negative effect on surface O_3 in eastern China.

Between the five strongest and five weakest SASM years during 1981–2019, O_3 concentrations decreased in eastern China, where surface O_3 concentrations have a maximum decrease of 5 ppb (10 %) in the strongest years compared to weakest years (Fig. 6). The impact of SASM1 is strong near the surface and gradually weakens with the increase of height

Table 2
The composite analyses of horizontal mass transport (Tg) of JJA O_3 from the surface to 500 hPa over south-central China (97.5°–117.5°E, 20°–35°N), eastern China (110°–117.5°E, 22°–34°N) and southern China (100°–117.5°E, 22°–32°N). The values are averaged over the selected five strongest and five weakest EASM, SASM1 and SASM2 years, respectively, and the differences are also calculated (strongest minus weakest). Positive values indicate incoming fluxes and negative values indicate outgoing fluxes.

	South-central China (97.5°–117.5°E, 20°–35°N)			Eastern China (110°–117.5°E, 22°–34°N)			Southern China (100°–117.5°E, 22°–32°N)		
	Strong	Weak	Differences	Strong	Weak	Differences	Strong	Weak	Differences
North	7.30	11.31	−4.01	−8.63	4.78	−13.41	−11.63	−12.94	1.31
South	3.60	1.55	2.05	12.45	8.55	3.90	8.57	14.58	−6.01
East	−8.34	−20.30	11.96	−19.09	−21.61	2.52	−6.29	−19.70	13.41
West	15.18	16.90	−1.72	14.32	11.87	2.45	8.45	14.90	−6.45

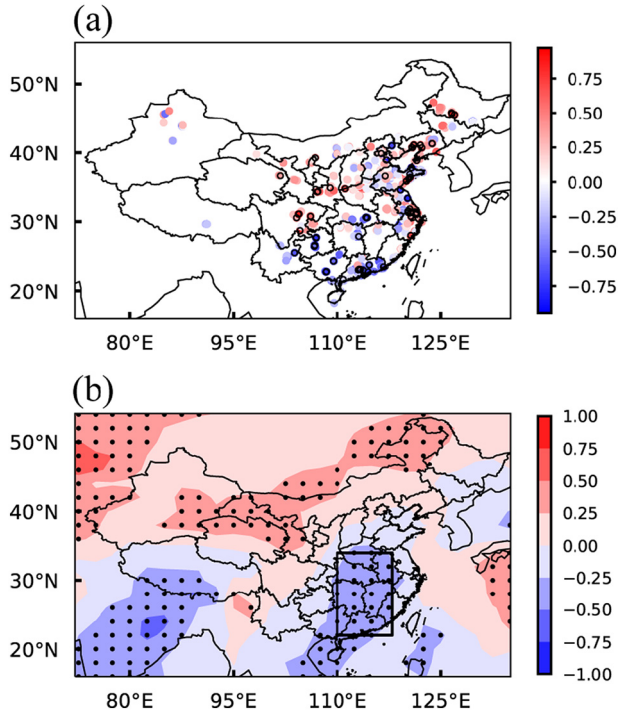

Fig. 5. Same as Fig. 2 but for the correlation coefficient between SASM1 index and JJA surface O_3 concentrations. Boxed area marks eastern China (110°–117.5°E, 22°–34°N).

(Fig. 6b and d). From June to August, the difference of O_3 concentration is the largest in July and August (Fig. S4), with O_3 concentrations in the strongest SASM1 years 5–10 ppb (10–20 %) lower than those in the weakest SASM1 years.

Fig. 7 shows the changes in summer meteorological parameters between the five strongest and five weakest SASM1 years. In the strongest SASM1 years, although the surface air temperature and downwelling shortwave radiation are higher than those in the weakest SASM1 year over the central part of eastern China (Fig. 7f and g), favoring the O_3 production, the abnormal southerlies at 850 hPa and 500 hPa blow the pollutant out of the northern boundary (Fig. 7a and b). It is verified by the IPR analysis that the horizontal transport process leads to the O_3 mass decrease at a rate of 6.84 Gg day^{-1}, largely offset by the increase in O_3 from the chemical production (5.16 Gg day^{-1}), diffusion and dry deposition processes (1.06 Gg day^{-1}) (Table 1), causing the net decrease in tropospheric O_3 concentrations over eastern China between the five strongest and five weakest SASM1 years. The horizontal mass budget shows that during the weakest SASM1 years O_3 was imported from the north of eastern China by 4.71 Tg in JJA (Table 2). However, due to the anomalous southerlies during the strongest SASM1 years, the import is reversed to export by 8.63 Tg, resulting in a net 13.41 Tg loss of O_3 through the north of eastern China, relative to the weakest years, and the net divergence of O_3 over eastern China.

4.2. Impacts of interannual variation in SASM2

Unlike the SASM1 index (35°–70°E, 2.5°–20°N), the SASM2 index is calculated as the average DNS over the sector (70°–110°E, 2.5°–20°N) near the

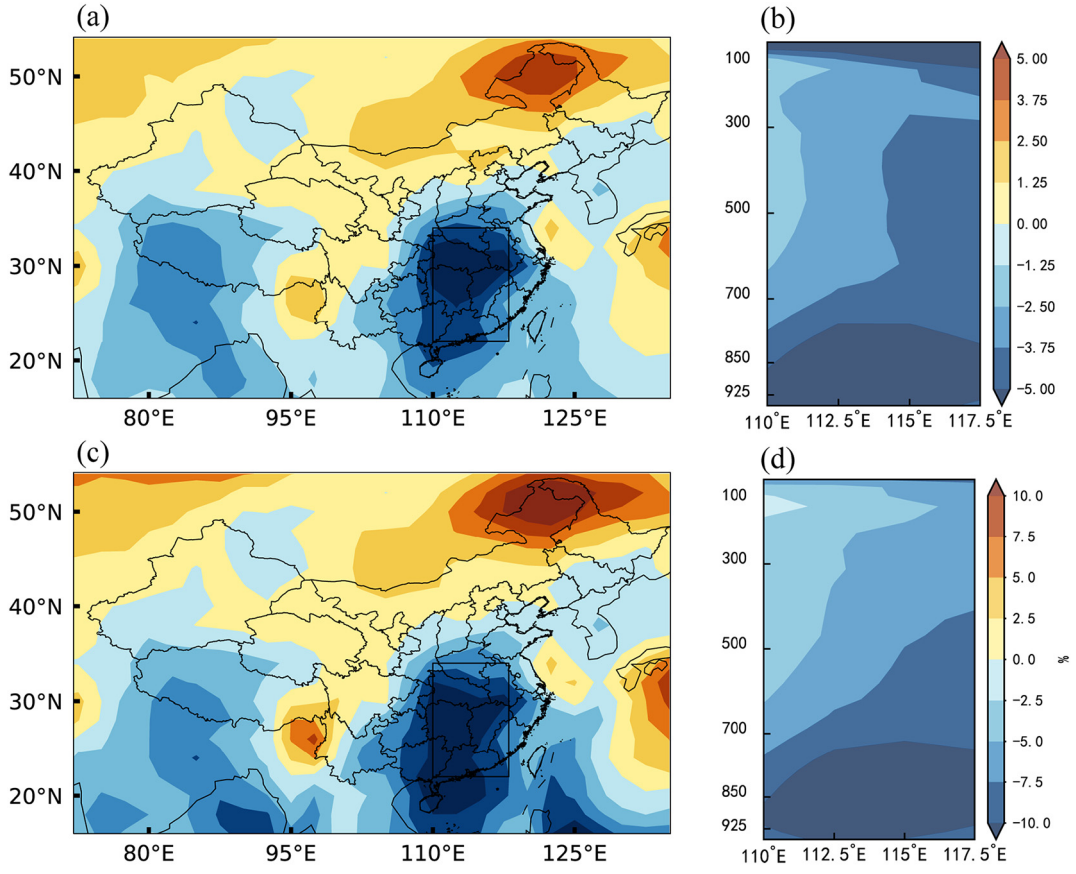

Fig. 6. Same as Fig. 3 but for the difference between the five strongest (1994, 1996, 2005, 2007 and 2017) and five weakest SASM1 years (2009, 2014, 2015, 2018 and 2019) (strongest minus weakest). Cross sections are averaged over 22°–34°N. Boxed area marks eastern China.

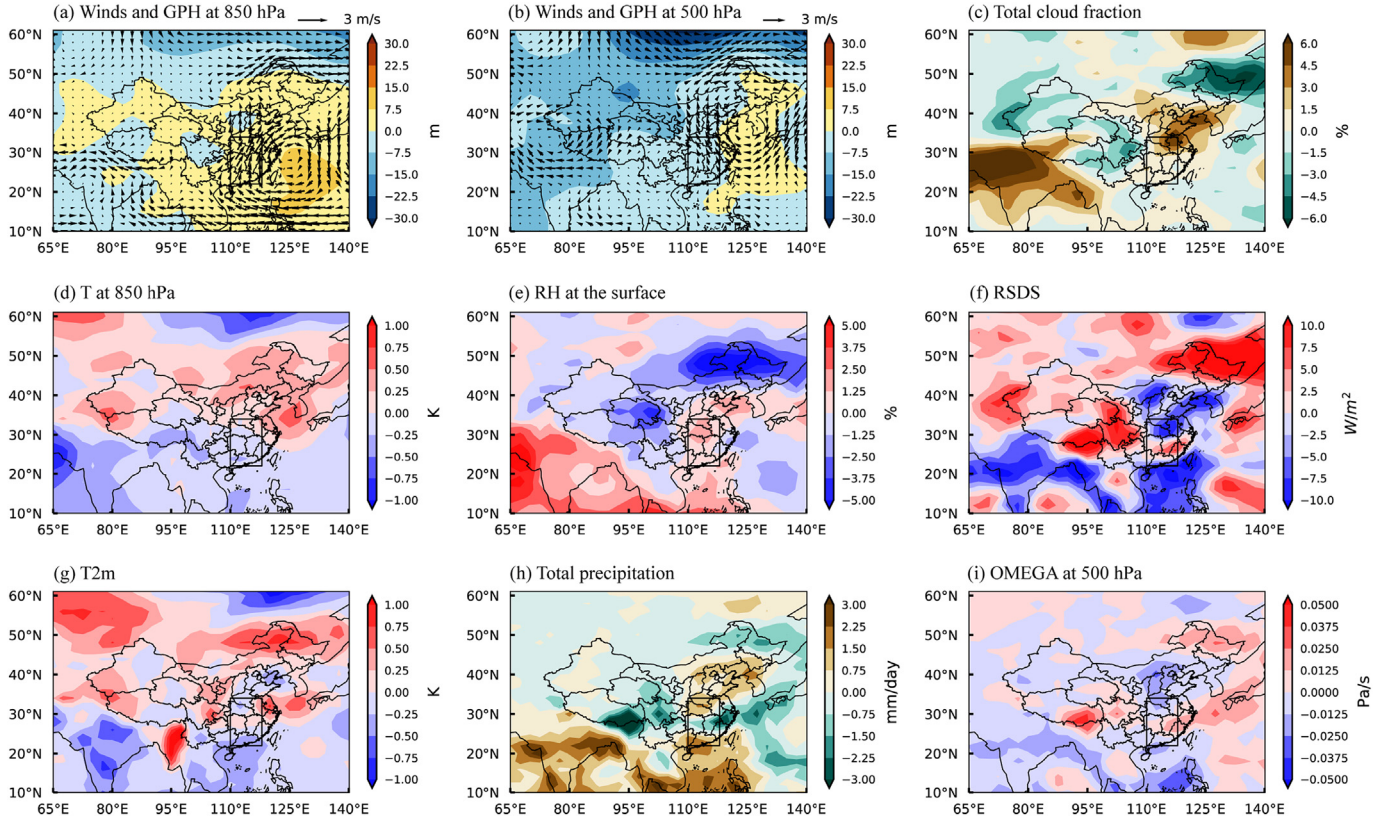

Fig. 7. Same as Fig. 4 but for the composite differences between five strongest and five weakest SASM1 years (strongest minus weakest). Boxed area marks eastern China.

EASM region (110°–140°E, 10°–40°N). The correlation coefficient between SASM2 index and EASM index is 0.82, whereas it is −0.23 between SASM1 index and EASM index, indicating that the SASM2 could have a similar impact on O_3 in China to that of EASM. As expected, the SASM2 index shows a significant positive correlation with modeled JJA surface O_3 concentrations over southern China and a negative correlation over the coastal areas and East China Sea during 1981–2019 (Fig. 8), with regional averaged correlation coefficient of 0.50 over southern China (100–117.5°E, 22–32°N). Observational data at 92 % (230 out of 250) sites exhibit positive correlation in southern China (Fig. S5), consistent with the simulations.

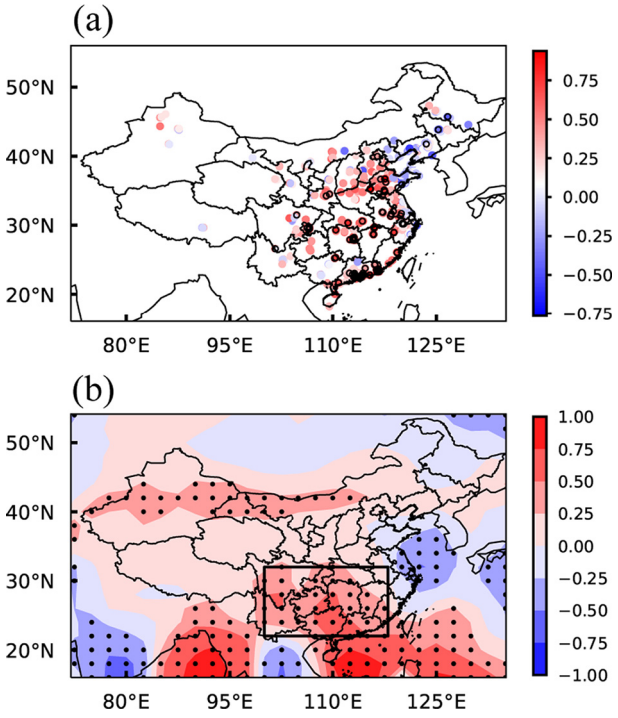

Fig. 8. Same as Fig. 2 but for the correlation coefficient between SASM2 index and JJA surface O_3 concentrations. Boxed area marks southern China (100°–117.5°E, 22°–32°N).

Between the five strongest and five weakest SASM2 years, the maximum changes in surface O_3 concentrations are higher than 5 ppb (10 %) over southern and southwestern China (Fig. 9a and c) and the biggest impact of SASM2 is around 850 and 600 hPa over southern China (Fig. 9b and d). Same as that of EASM, the influence of SASM2 on O_3 in China is the strongest in August during summer (Fig. S6), presumably related to the timing of the monsoon retreat (Lu et al., 2018).

The composite differences in meteorological parameters between the five strongest and five weakest years of SASM2 (Fig. 10) are similar to those of EASM years (Fig. 4). The anomalous northeasterlies reduce the export of O_3 from the east of the southern China, leading to the O_3 convergence and thus increase in O_3 concentrations over this region, although the decrease in temperature and increase in humidity weaken the photochemical production of O_3.

5. Future variations in monsoon strength

To explore the future changes in summertime O_3 in China influenced by the ASM systems, Fig. 11 displays the future variations during 2015–2100 in EASM, SASM1 and SASM2 indices calculated using the CMIP6 future projections with various climate policy scenarios (SSP1-2.6, SSP2-4.5, SSP3-7.0 and SSP5-8.5). Under sustainable and intermediate development scenarios (SSP1-2.6 and SSP2-4.5), EASM and SASM1 intensities do not show an obvious trend in the future, but the SASM2 intensity is projected to decrease during 2015–2100. Considering the positive relationship between SASM2 index and O_3 concentration in southern China, it indicates that the sustainable and medium development scenarios are the perfect

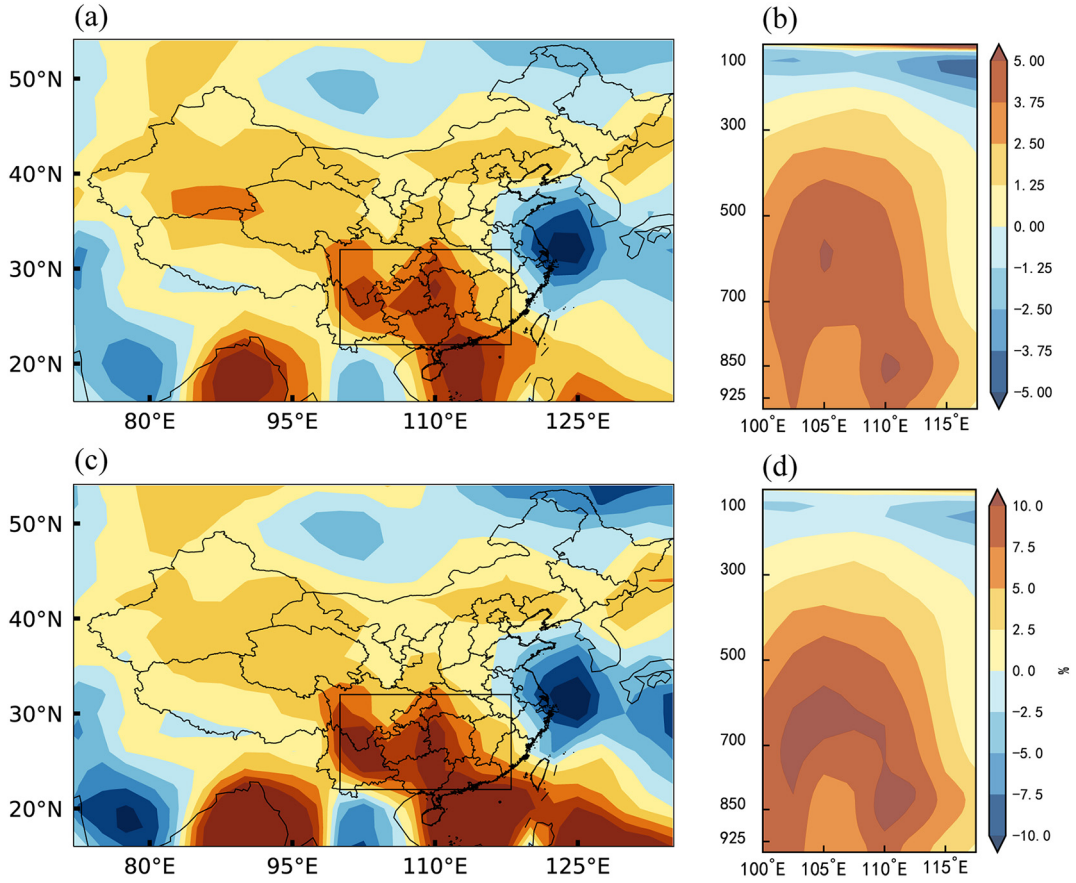

Fig. 9. Same as Fig. 3 but for the difference between the five strongest (1985, 1990, 1994, 2001 and 2018) and five weakest SASM2 years (1988, 1996, 1998, 2007 and 2010) (strongest minus weakest). Cross sections are averaged over 22°–32°N. Boxed area marks southern China.

pathways that can help to mitigate O_3 pollution in China through changing monsoon strength.

Under high social vulnerability and radiative forcing scenarios (SSP3-7.0 and SSP5-8.5), both the SASM1 and SASM2 indices show similar trends that firstly decrease than keep stable or increase, which effects on O_3 may offset each other although the regions they affect are relatively different. However, EASM strength slightly increases after 2040 in SSP3-7.0 and shows a rapid growth since 2065 in SSP5-8.5. The intensified EASM in the future is also reported by Wu et al. (2022). Since that EASM has a strong positive correlation with O_3 concentration in south-central China, the future increase in EASM intensity suggests that high anthropogenic radiative forcing and social vulnerability could enhance future O_3 pollution in China in the perspective of monsoon systems.

6. Conclusions and discussions

Increasingly serious O_3 pollution endangers human health and ecosystems in China. This study quantifies the effects of ASM (including both EASM and SASM) on O_3 concentrations during summer in China and reveals the influencing mechanisms, based on surface O_3 measurements from 2014 to 2020 and simulated O_3 data by the global atmospheric chemistry model GEOS-Chem over 1981–2019, which have important implications for air pollution prevention and mitigation in China.

A significant positive correlation between the EASM index and summer surface O_3 concentrations in south-central China with a correlation coefficient of 0.6. Compared to the selected five weakest EASM years, O_3 levels were generally higher in the five strongest EASM years in south-central China, with a maximum difference above 5 ppb (10 % relative to the mean). Composite analysis of meteorological parameters shows that the decrease in prevailing southwesterlies along with the weakened WPSH in south-central China during the strongest EASM years, relative to the weakest years, reduce the export of polluted air from the east of south-central China. The O_3 mass budget analysis confirms that the weakened transboundary transport leads to the O_3 convergence and thus the increase in tropospheric O_3 concentrations during the strongest EASM years, although the low temperature and high humidity are not conducive to the local chemical production of O_3.

As the other important component of the ASM, SASM can be further divided into two components that have different linkages and locations within the SASM. The SASM2 sector near East Asia has a similar impact on O_3 in southern China (correlation coefficient of 0.50) to that of EASM. O_3 concentrations in southern China are higher in the strongest SASM2 years with a maximum difference of 5 ppb (10 %) than the weakest SASM2 years, and the O_3 convergence due to weakened southwesterlies can also explain the concentration increases. In contrast, the intensity of the SASM1 is negatively correlated with surface O_3 concentrations in eastern China (correlation coefficient of -0.40) and the maximum difference in surface O_3 concentration is 5 ppb (10 %) between the five strong and the five weakest SASM1 years. Relative to the weakest years, although the increases in surface air temperature and downwelling short-wave radiation in the strongest SASM1 years are favorable for O_3 production, anomalous southerlies transport pollutants out of the region from the northern boundary, resulting in a net decline in O_3 concentrations in eastern China.

Future projections in ASM from CMIP6 simulations suggest that the sustainable and medium development scenarios are the perfect pathways that can help to mitigate O_3 pollution in China, while high social vulnerability and radiative forcing scenarios could enhance future O_3 pollution in China, in the perspective of changing monsoon systems.

The impacts of EASM on the interannual changes in O_3 in China have also been examined in previous studies using model simulations alone for

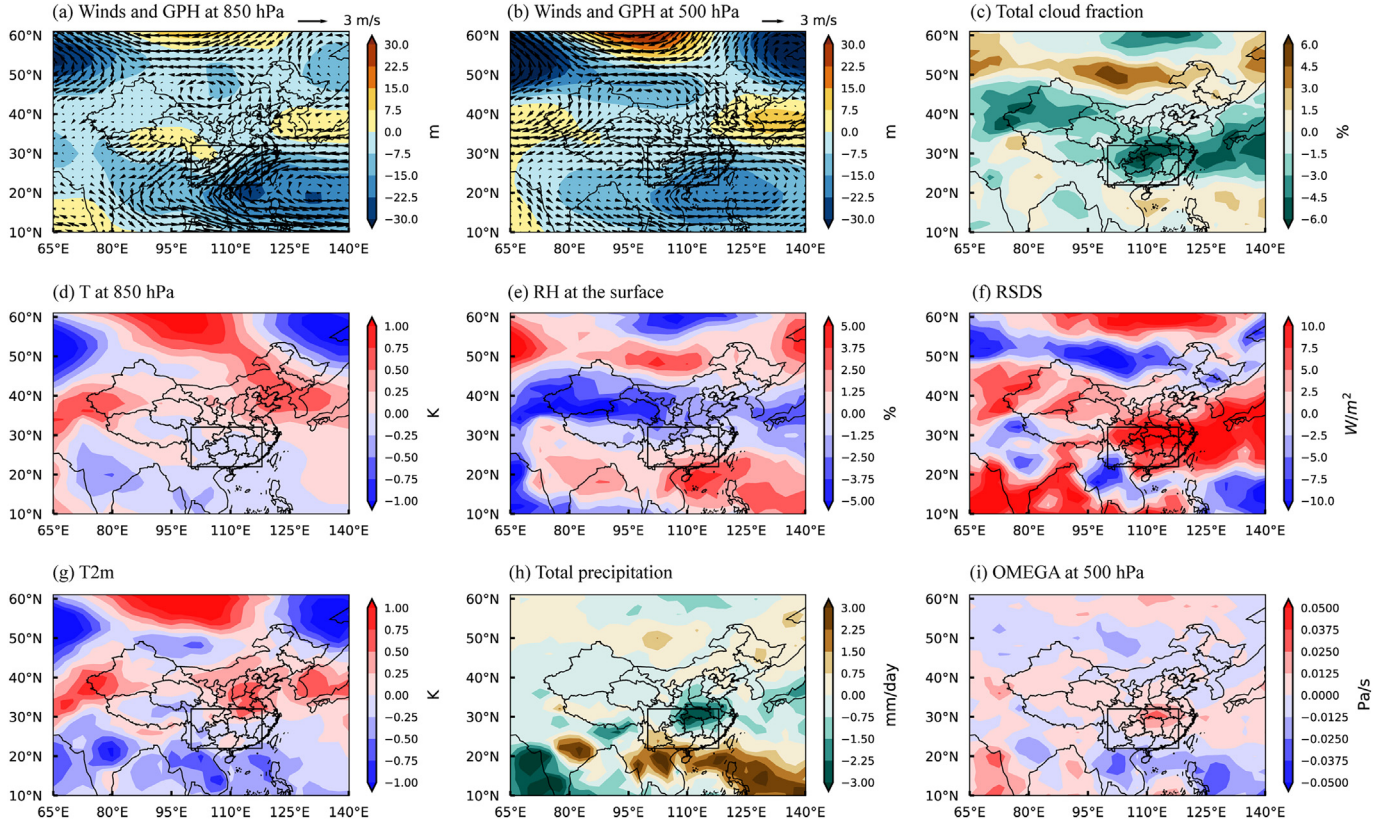

Fig. 10. Same as Fig. 4 but for the composite differences between five strongest and five weakest SASM2 years (strongest minus weakest).

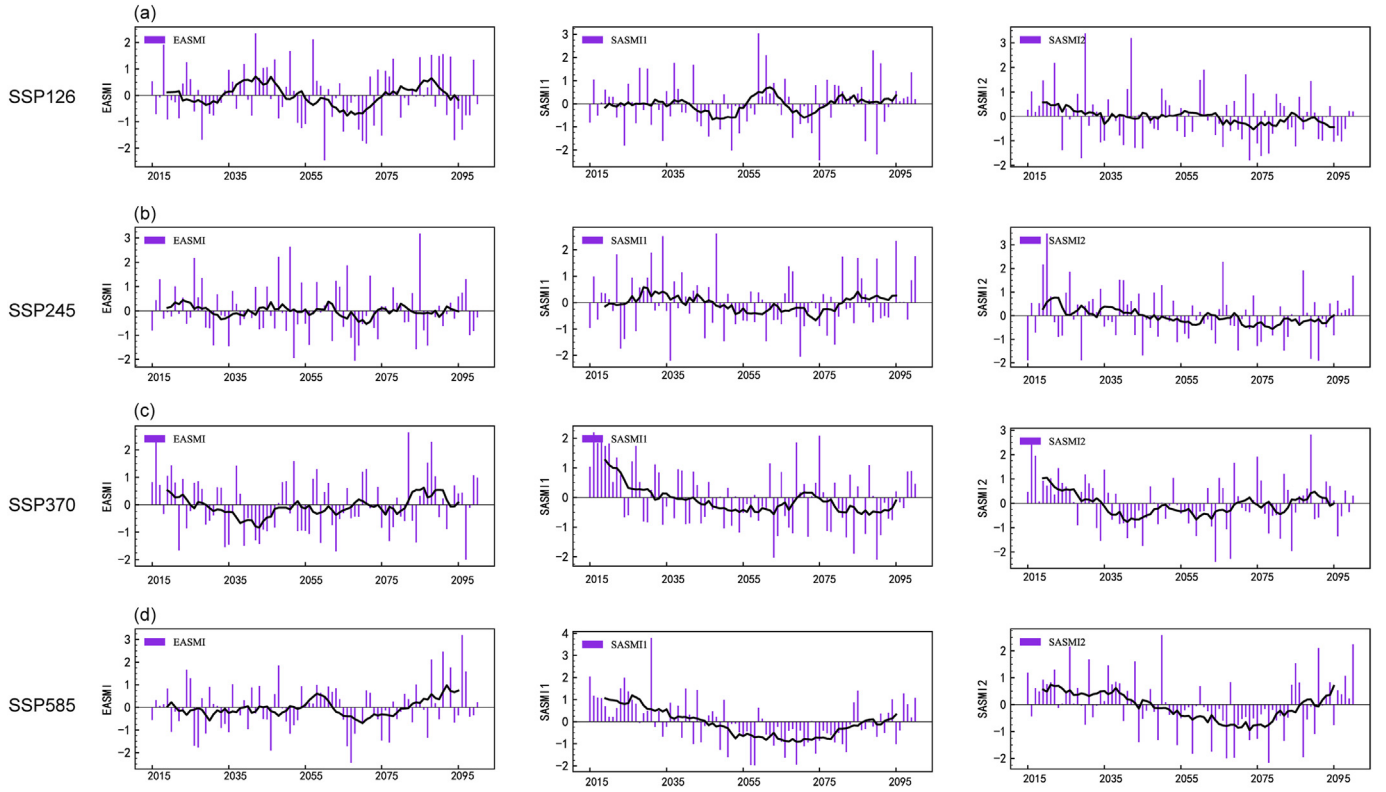

Fig. 11. Time series of EASM index (left column), SASM1 index (middle column) and SASM2 index (right column) calculated based on the CMIP6 multi-model results under (a) SSP1-2.6, (b) SSP2-4.5, (c) SSP3-7.0 and (d) SSP5-8.5 scenarios over 2015–2100 (bars), with solid black lines representing the 10-year moving average.

a short time period or with surface observations at individual sites. This study quantifies the influences of both EASM and SASM on O_3 concentrations with 39-year model simulations, together with O_3 measurements from the nation-wide observational network. The results suggest that the ASM has an important impact on the interannual variation in JJA O_3 concentrations in China, through changing transboundary transport of O_3 related to the variability of large-scale circulations.

The finding of a summer O_3 concentration increase in strong EASM years is consistent with several previous studies (Li et al., 2017; Yang et al., 2014; Zhou et al., 2013). Li et al. (2017) considered the vertical turbulence and advection and chemical production as the main processes influenced by EASM, but we show that regional O_3 changes are primarily due to the changes in transboundary transport of O_3. The differences could be due to many reasons, including the non-linear relationship between O_3 and its precursors, lack of representation of transboundary transport of O_3 from regions outside of the domain in regional models, different physical and chemical treatments between the two models, lack of some natural emissions in Li et al. (2017) and coarse model resolution in this study. Xu et al. (2018) reported a negative correlation between EASM and O_3 concentrations in July and a weak correlation in June and August at Mt. Waliguan Observatory on the Tibetan Plateau over 1994–2013, while we show an insignificant relationship between EASM and JJA O_3 concentration at this site.

Natural emissions, such as biogenic VOCs (BVOCs) and soil NO_x, play important roles in O_3 formation (Fu et al., 2019; Lu et al., 2019a, 2019b). Emissions of BVOCs from plants vary greatly between species and are non-linear depending on factors such as sunlight, temperature, and soil moisture (Fu et al., 2019; Hantson et al., 2017; Jiang et al., 2018; Wang et al., 2018; Weaver et al., 2009). Fixing BVOCs during simulations could lead to a bias in the O_3 chemical production in different monsoon years. Variations in soil NO_x emissions owing to the changes in meteorology in different monsoon years further modulate O_3 (Lu et al., 2019a, 2019b; Romer et al., 2018; Yan et al., 2005). However, due to the complexity and uncertainty in the response of O_3 pollution to natural emissions, the potential impact of fixing natural emissions on O_3 concentrations in China requires further exploration in the future studies.

Owing to the complexity of the factors influencing surface O_3, in future studies, it is better to obtain more observational O_3 data confirming the relationship between ASM and O_3 in future studies. The model simulations could also be improved at a finer horizontal resolution. As well as taking into account other factors such as variability in natural emissions, it is important to note that other modes of climate variability such as El Niño can also have an impact on surface O_3 in China. Yang et al. (2022) found a positive correlation between summer surface O_3 concentration in China and ENSO index during 1990–2019, with a 20 % maximum increase in O_3 concentrations in southern China in El Niño relative to La Niña years and suggested that the ENSO impacts are also associated with monsoonal changes. Therefore, the synergistic impacts of monsoon and other climate phenomenon on O_3 in China warrant further investigation.

CRediT authorship contribution statement

Yang Zhou: Conceptualization, Data curation, Formal analysis, Investigation, Methodology, Software, Visualization, Writing – original draft. **Yang Yang**: Conceptualization, Data curation, Formal analysis, Project administration, Supervision, Writing – review & editing. **Hailong Wang**: Formal analysis, Writing – review & editing. **Jing Wang**: Formal analysis. **Mengyun Li**: Data curation. **Huimin Li**: Data curation. **Pinya Wang**: Formal analysis. **Jia Zhu**: Formal analysis. **Ke Li**: Formal analysis. **Hong Liao**: Writing – review & editing.

Data availability

The GEOS-Chem model is available at http://acmg.seas.harvard.edu/geos/(last access: June 2022). O_3 observations over China can be obtained from the China National Environmental Monitoring Centre (http://www.cnemc.cn, last access: June 2022). MERRA-2 reanalysis data can be downloaded at https://gmao.gsfc.nasa.gov/reanalysis/MERRA-2/ (last access: June 2022). The multi-model future simulations of the Coupled Model Intercomparison Project Phase 6 (CMIP6) are from https://esgf-node.llnl.gov/search/cmip6/ (last access: June 2022).

Declaration of competing interest

The authors declare that they have no known competing financial interests or personal relationships that could have appeared to influence the work reported in this paper.

Acknowledgments

This study was supported by the National Key Research and Development Program of China (grant 2020YFA0607803 and 2019YFA0606800), the National Natural Science Foundation of China (grant 41975159) and Jiangsu Science Fund for Distinguished Young Scholars (grant BK20211541). HW acknowledges the support by the U.S. Department of Energy (DOE), Office of Science, Office of Biological and Environmental Research (BER), as part of the Earth and Environmental System Modeling program. The Pacific Northwest National Laboratory (PNNL) is operated for DOE by the Battelle Memorial Institute under contract DE-AC05-76RLO1830.

Appendix A. Supplementary data

Supplementary data to this article can be found online at https://doi.org/10.1016/j.scitotenv.2022.157785.

References

Ainsworth, E.A., Yendrek, C.R., Sitch, S., Collins, W.J., Emberson, L.D., 2012. The effects of tropospheric ozone on net primary productivity and implications for climate change. Annu. Rev. Plant Biol. 63, 637–661. https://doi.org/10.1146/annurev-arplant-042110-103829.

Chen, K., Fiore, A.M., Chen, R., Jiang, L.W., Jones, B., Schneider, A., Peters, A., Bi, J., Kan, H.L., Kinney, P.L., 2018. Future ozone-related acute excess mortality under climate and population change scenarios in China: a modeling study. PLoS Med. 15, e1002598. https://doi.org/10.1371/journal.pmed.1002598.

Ding, Y., Chan, J.C.L., 2005. The East Asian summer monsoon: an overview. Meteorog. Atmos. Phys. 89, 117–142. https://doi.org/10.1007/s00703-005-0125-z.

Emberson, L.D., Pleijel, H., Ainsworth, E.A., Maurits B., van, Osborne, S., Mills, G., Pandey, D., Dentener, F., Büker, P., Ewert, F., Koeble, R., Rita D., van, 2018. Ozone effects on crops and consideration in crop models. Eur. J. Agron. 100, 19–34. https://doi.org/10.1016/j.eja.2018.06.002.

Fu, Y., Liao, H., Yang, Y., 2019. Interannual and decadal changes in tropospheric ozone in China and the associated chemistry-climate interactions: a review. Adv. Atmos. Sci. 36, 975–993. https://doi.org/10.1007/s00376-019-8216-9.

Gao, M., Gao, J., Zhu, B., Kumar, R., Lu, X., Song, S., Zhang, Y., Jia, B., Wang, P., Beig, G., Hu, J., Ying, Q., Zhang, H., Sherman, P., McElroy, M.B., 2020. Ozone pollution over China and India: seasonality and sources. Atmos. Chem. Phys. 20, 4399–4414. https://doi.org/10.5194/acp-20-4399-2020.

Gong, C., Liao, H., Zhang, L., Yue, X., Dang, R., Yang, Y., 2020. Persistent ozone pollution episodes in North China exacerbated by regional transport. Environ. Pollut. 265, 115056. https://doi.org/10.1016/j.envpol.2020.115056.

Guenther, A.B., Jiang, X., Heald, C.L., Sakulyanontvittaya, T., Duhl, T., Emmons, L.K., Wang, X., 2012. The model of emissions of gases and aerosols from nature version 2.1 (MEGAN2.1): an extended and updated framework for modeling biogenic emissions. Geosci. Model Dev. 5, 1471–1492. https://doi.org/10.5194/gmd-5-1471-2012.

Hantson, S., Knorr, W., Schurgers, G., Tam, P., Arneth, A., 2017. Global isoprene and monoterpene emissions under changing climate, vegetation, CO2 and land use. Atmos. Environ. 155, 35–45. https://doi.org/10.1016/j.atmosenv.2017.02.010.

He, J., Ju, J., Wen, Z., Lu, J.M., Jin, Q.H., 2007. A review of recent advances in research on Asian monsoon in China. Adv. Atmos. Sci. 24, 972–992. https://doi.org/10.1007/s00376-007-0972-2.

Hoesly, R.M., Smith, S.J., Feng, L., Klimont, Z., Janssens-Maenhout, G., Pitkanen, T., Seibert, J.J., Vu, L., Andres, R.J., Bolt, R.M., Bond, T.C., Dawidowski, L., Kholod, N., Kurokawa, J.I., Li, M., Liu, L., Lu, Z., Moura, M.C.P., O'Rourke, P.R., Zhang, Q., 2018. Historical (1750–2014) anthropogenic emissions of reactive gases and aerosols from the community emissions data system (CEDS). Geosci. Model Dev. 11, 369–408. https://doi.org/10.5194/gmd-11-369-2018.

Hudman, R.C., Moore, N.E., Mebust, A.K., Martin, R.V., Russell, A.R., Valin, L.C., Cohen, R.C., 2012. Steps towards a mechanistic model of global soil nitric oxide emissions:

implementation and space based-constraints. Atmos. Chem. Phys. 12, 7779–7795. https://doi.org/10.5194/acp-12-7779-2012.
Jiang, X.Y., Guenther, A., Potosnak, M., Geron, C., Seco, R., Karl, T., Kim, S., Gu, L.H., Pallardy, S., 2018. Isoprene emission response to drought and the impact on global atmospheric chemistry. Atmos. Environ. 183, 69–83. https://doi.org/10.1016/j.atmosenv.2018.01.026.
Li, J.P., Zeng, Q.C., 2002. A unified monsoon index. Geophys. Res. Lett. 29, 1274. https://doi.org/10.1029/2001GL013874.
Li, K., Jacob, D.J., Liao, H., Qiu, Y., Shen, L., Zhai, S., Bates, K.H., Sulprizio, M.P., Song, S., Lu, X., Zhang, Q., Zheng, B., Zhang, Y., Zhang, J., Lee, H.C., Kuk, S.K., 2021. Ozone pollution in the North China plain spreading into the late-winter haze season. Proc. Natl. Acad. Sci. U. S. A. 118, 1–7. https://doi.org/10.1073/pnas.2015797118.
Li, K., Jacob, D.J., Liao, H., Shen, L., Zhang, Q., Bates, K.H., 2019. Anthropogenic drivers of 2013–2017 trends in summer surface ozone in China. Proc. Natl. Acad. Sci. U. S. A. 116, 422–427. https://doi.org/10.1073/pnas.1812168116.
Li, S., Wang, T., Huang, X., Pu, X., Li, M., Chen, P., Wang, M., 2017. Impact of East Asian summer monsoon on surface ozone pattern in China. J. Geophys. Res. Atmos. 123, 1401–1411. https://doi.org/10.1002/2017JD027190.
Lin, J.T., McElroy, M.B., 2010. Impacts of boundary layer mixing on pollutant vertical profiles in the lower troposphere: implications to satellite remote sensing. Atmos. Environ. 44, 1726–1739. https://doi.org/10.1016/j.atmosenv.2010.02.009.
Liu, N.W., Lin, W.L., Ma, J.Z., 2019. Seasonal variation in surface ozone and its regional characteristics at global atmosphere watch stations in China. J. Environ. Sci. 77, 291–302. https://doi.org/10.1016/j.jes.2018.08.009.
Lu, X., Zhang, L., Wang, X., Gao, M., Li, K., Zhang, Y., Yue, X., Zhang, Y., 2020. Rapid increases in warm-season surface ozone and resulting health impact in China since 2013. Environ. Sci. Technol. Lett. 7, 240–247. https://doi.org/10.1021/acs.estlett.0c00171.
Lou, S., Liao, H., Yang, Y., Mu, Q., 2015. Simulation of the interannual variations of tropospheric ozone over China: roles of variations in meteorological parameters and anthropogenic emissions. Atmos. Environ. 122, 839–851. https://doi.org/10.1016/j.atmosenv.2015.08.081.
Lu, X., Zhang, L., Chen, Y., Zhou, M., Zheng, B., Li, K., Liu, Y., Lin, J., Fu, T.M., Zhang, Q., 2019. Exploring 2016–2017 surface ozone pollution over China: source contributions and meteorological influences. Atmos. Chem. Phys. 19, 8339–8361. https://doi.org/10.5194/acp-19-8339-2019.
Lu, X., Zhang, L., Liu, X., Gao, M., Zhao, Y.H., Shao, J.Y., 2018. Lower tropospheric ozone over India and its linkage to the South Asian monsoon. Atmos. Chem. Phys. 18, 3101–3118. https://doi.org/10.5194/acp-18-3101-2018.
Lu, X., Zhang, L., Shen, L., 2019. Meteorology and climate influences on tropospheric ozone: a review of natural sources, chemistry, and transport patterns. Curr. Pollut. Rep. 5, 238–260. https://doi.org/10.1007/s40726-019-00118-3.
Malley, C.S., Henze, D.K., Kuylenstierna, J.C.I., Vallack, H.W., Davila, Y., Anenberg, S.C., Turner, M.C., Ashmore, M.R., 2017. Updated global estimates of respiratory mortality in adults ≥30 years of age attributable to long-term ozone exposure. Environ. Health Perspect. 125, 087021. https://doi.org/10.1289/ehp1390.
Mao, J.Q., Paulot, F., Jacob, D.J., Cohen, R.C., Crounse, J.D., Wennberg, P.O., Keller, C.A., Hudman, R.C., Barkley, M.P., Horowitz, L.W., 2013. Ozone and organic nitrates over the eastern United States: sensitivity to isoprene chemistry. J. Geophys. Res. Atmos. 118, 11256–11268. https://doi.org/10.1002/jgrd.50817.
McLinden, C.A., Olsen, S.C., Hannegan, B., Wild, O., Prather, M.J., Sundet, J., 2000. Stratospheric ozone in 3-D models: a simple chemistry and the cross-tropopause flux. J. Geophys. Res. Atmos. 105, 14653–14665. https://doi.org/10.1029/2000jd900124.
Mills, G., Pleijel, H., Malley, C.S., Sinha, B., Cooper, O.R., Schultz, M.G., Neufeld, H.S., Simpson, D., Sharps, K., Feng, Z., Gerosa, G., Harmens, H., Kobayashi, K., Saxena, P., Paoletti, E., Sinha, V., Xu, X., 2018. Tropospheric ozone assessment report: present-day tropospheric ozone distribution and trends relevant to vegetation. Elem. Sci. Anth. 6, 47. https://doi.org/10.1525/elementa.302.
Mu, Q., Liao, H., 2014. Simulation of the interannual variations of aerosols in China: role of variations in meteorological parameters. Atmos. Chem. Phys. 14, 9597–9612. https://doi.org/10.5194/acp-14-9597-2014.
Ni, R., Lin, J., Yan, Y., Lin, W., 2018. Foreign and domestic contributions to springtime ozone over China. Atmos. Chem. Phys. 18, 11447–11469. https://doi.org/10.5194/acp-18-11447-2018.
Ott, L.E., Pickering, K.E., Stenchikov, G.L., Allen, D.J., DeCaria, A.J., Ridley, B., Lin, R.-F., Lang, S., Tao, W.-K., 2010. Production of lightning NOx and its vertical distribution calculated from three-dimensional cloud-scale chemical transport model simulations. J. Geophys. Res. 115, D04301. https://doi.org/10.1029/2009JD011880.
Pye, H.O., Liao, H., Wu, S., Mickley, L.J., Jacob, D.J., Henze, D.K., Seinfeld, J.H., 2009. Effect of changes in climate and emissions on future sulfate-nitrate-ammonium aerosol levels in the United States. J. Geophys. Res. 114, D01205. https://doi.org/10.1029/2008JD010701.
Romer, P.S., Duffey, K.C., Wooldridge, P.J., Edgerton, E., Baumann, K., Feiner, P.A., Miller, D.O., Brune, W.H., Koss, A.R., de Gouw, J.A., Misztal, P.K., Goldstein, A.H., Cohen, R.C., 2018. Effects of temperature-dependent NOx emissions on continental ozone production. Atmos. Chem. Phys. 18, 2601–2614. https://doi.org/10.5194/acp-18-2601-2018.
Sherwen, T., Schmidt, J.A., Evans, M.J., Carpenter, L.J., Großmann, K., Eastham, S.D., Jacob, D.J., Dix, B., Koenig, T.K., Sinreich, R., Ortega, I., Volkamer, R., Saiz-Lopez, A., Prados-Roman, C., Mahajan, A.S., Ordóñez, C., 2016. Global impacts of tropospheric halogens (Cl, Br, I) on oxidants and composition in GEOS-Chem. Atmos. Chem. Phys. 16, 12239–12271. https://doi.org/10.5194/acp-16-12239-2016.
Shu, L., Xie, M., Wang, T., Gao, D., Chen, P., Han, Y., Li, S., Zhuang, B., Li, M., 2016. Integrated studies of a regional ozone pollution synthetically affected by subtropical high and typhoon system in the Yangtze River Delta region, China. Atmos. Chem. Phys. 16, 15801–15819. https://doi.org/10.5194/acp-16-15801-2016.
Steinke, S., Chiu, H.Y., Yu, P.S., Shen, C.C., Erlenkeuser, H., Löwemark, L., Chen, M.T., 2006. On the influence of sea level and monsoon climate on the southern South China Sea freshwater budget over the last 22,000 years. Quat. Sci. Rev. 25, 1475–1488. https://doi.org/10.1016/j.quascirev.2005.12.008.
van der Werf, G.R., Randerson, J.T., Giglio, L., van Leeuwen, T.T., Chen, Y., Rogers, B.M., Mu, M., van Marle, M.J.E., Morton, D.C., Collatz, G.J., Yokelson, R.J., Kasibhatla, P.S., 2017. Global fire emissions estimates during 1997–2016. Earth Syst. Sci. Data 9, 697–720. https://doi.org/10.5194/essd-9-697-2017.
Wang, B., Shuman, J., Shugart, H.H., Lerdau, M.T., 2018. Biodiversity matters in feedbacks between climate change and air quality: a study using an individual-based model. Ecol. Appl. 28, 1223–1231. https://doi.org/10.1002/eap.1721.
Wang, B., Xiang, B., Lee, J.-Y., 2013. Subtropical high predictability establishes a promising way for monsoon and tropical storm predictions. Proc. Natl. Acad. Sci. U. S. A. 110, 2718–2722. https://doi.org/10.1073/pnas.1214626110.
Weaver, C.P., Liang, X.Z., Zhu, J., Adams, P.J., Amar, P., Avise, J., 2009. A preliminary synthesis of modeled climate change impacts on us regional ozone concentrations. Bull. Am. Meteorol. Soc. 90, 1843–1863. https://doi.org/10.1175/2009bams2568.1.
Wu, Q.Y., Li, Q.Q., Ding, Y.H., Shen, X.Y., Zhao, M.C., Zhu, Y.X., 2022. Asian summer monsoon responses to the change of land–sea thermodynamic contrast in a warming climate: CMIP6 projections. Adv. Clim. Chang. Res. 13, 205–217. https://doi.org/10.1016/j.accre.2022.01.001.
Xu, W., Xu, X., Lin, M., Lin, W., Tarasick, D., Tang, J., Ma, J., Zheng, X., 2018. Long-term trends of surface ozone and its influencing factors at the mt waliguan GAW station, China-part 2: the roles of anthropogenic emissions and climate variability. Atmos. Chem. Phys. 18, 773–798. https://doi.org/10.5194/acp-18-773-2018.
Yan, X., Ohara, T., Akimoto, H., 2005. Statistical modeling of global soil NOx emissions. Glob Biogeochem. Cycles. 19, GB3019. https://doi.org/10.1029/2004gb002276.
Yang, Y., Liao, H., Li, J., 2014. Impacts of the East Asian summer monsoon on interannual variations of summertime surface-layer ozone concentrations over China. Atmos. Chem. Phys. 14, 6867–6880. https://doi.org/10.5194/acp-14-6867-2014.
Yang, Y., Li, M., Wang, H., Li, H., Wang, P., Li, K., Gao, M., Liao, H., 2022. ENSO modulation of summertime tropospheric ozone over China. Environ. Res. Lett. 17, 034020. https://doi.org/10.1088/1748-9326/ac54cd.
Yin, X.F., Kang, S.C., Foy, B., 2017. Surface ozone at Nam Co in the inland tibetan plateau: variation, synthesis comparison and regional representativeness. Atmos. Chem. Phys. 17, 11293–11311. https://doi.org/10.5194/acp-17-11293-2017.
Zhao, C., Wang, Y., Yang, Q., Fu, R., Cunnold, D., Choi, Y., 2010. Impact of east asian summer monsoon on the air quality over China: view from space. J. Geophys. Res. 115, D09301. https://doi.org/10.1029/2009JD012745.
Zhou, D.R., Ding, A.J., Mao, H.T., 2013. Impacts of the East Asian monsoon on lower tropospheric ozone over coastal South China. Environ. Res. Lett. 8, 044011. https://doi.org/10.1088/1748-9326/8/4/044011.